1-30-2007

High Temperature Heat Exchanger Project: Quarterly Progress Report October 1, 2006 through December 31, 2006

Anthony Hechanova
University of Nevada, Las Vegas, hechanova@unlv.nevada.edu

High Temperature Heat Exchanger Project

Under Financial Assistance
DE-FC07-04ID14566
Awarded by the United States of America Acting Through the
United States Department of Energy

Quarterly Progress Report
October 1, 2006 through December 31, 2006

The UNLV Research Foundation
4505 Maryland Parkway
P. O. Box 452036
Las Vegas, NV 89154-2036

Anthony E. Hechanova, Ph.D.
Project Manager
(702) 895-1457
(702) 895-2354 (FAX)
hechanova@unlv.nevada.edu

January 30, 2007

UNLV Research Foundation
High Temperature Heat Exchanger (HTHX) Project
Quarterly Report (October 1, 2006 to December 31, 2006)

Contents

1.0 UNLV Design and Testing Group

1.1 HTHX Thermal Systems Design (PI: Yitung Chen, UNLV)

1.1.1 HTHX Thermal Systems Design Highlights

- Modifications to the single-channel models of the Ceramatec heat exchanger and decomposer concept for hexagonal flow channels under two values of layer-overlapping (50% and 100%) and for diamond-shaped flow channels were completed.
- The finite element calculations of the "Ball on Three Ball Test" for ceramic material for the purpose of selecting the appropriate specimen thickness for future experimental testing was performed for plate thicknesses ranging from 2 to 8 mm.
- A finite element model of the "Ball on Three Ball Test" was also studied for discs having micro-channels.
- A two-dimensional axisymmetric model of bayonet heat exchanger and decomposer design provided by Sandia design was developed.
- A parametric study of the bayonet heat exchanger and decomposer was performed.
- A two-dimensional numerical model using axisymmetric geometry of shell-and-tube type heat exchanger and decomposer was studied. A mesh independence study for the flow with a porous media zone (simulating a catalytic packed bed) was completed.

1.1.2 HTHX Thermal Systems Design Technical Summary

Numerical Analyses with Chemical Reactions and Optimization Studies for Ceramatec Sulfuric Acid Decomposer

Modifications of to the single-channel models of Ceramatec heat exchanger and decomposer concept for hexagonal layers under two values of layer-overlapping (50% and 100%) and for diamond-shaped layers were completed. The interface zones used in the models were removed. As result of the interface zone removal, the number of computational nodes and cells was increased 3-4 times and the required convergence time for the energy equation was decreased approximately 10 times.

Calculations of the Arrhenius constants (activation energy E_a and pre-exponential factor A_r) were performed based on the INL experimental measurement data from the catalytic packed bed decomposer. The experimental work was conducted by Dan Ginosar at INL. The calculated constants are:

E_a=32670.69 J/mol and A_r=1274.5 s^{-1} for 1% Pt loaded into TiO_2 support

E_a= 46240.37 J/mol and A_r= 9142.7 s^{-1} for 0.1% Pt loaded into TiO_2 support.

The activation energy is consistent with data from the literature. The pre-exponential factor is much smaller as compared with the experimental data calculated by other authors. The reason for the discrepancy may be the difference in the operating conditions.

The results of the numerical calculations with a surface chemical reaction (SO_3=SO_2+0.5O_2) in the packed bed region were compared with experimental data obtained by Ginosar at INL. The comparison was done for 0.1% Pt loaded into a TiO_2 support. The numerical and experimental data have good agreement (see Figure 1). The difference in sulfur trioxide decomposition between numerical and experimental data is within 20% for the temperature range 700-900ºC. This investigation was completed for benchmarking the chemical reaction model which is used for Ceramatec sulfuric acid decomposer calculations.

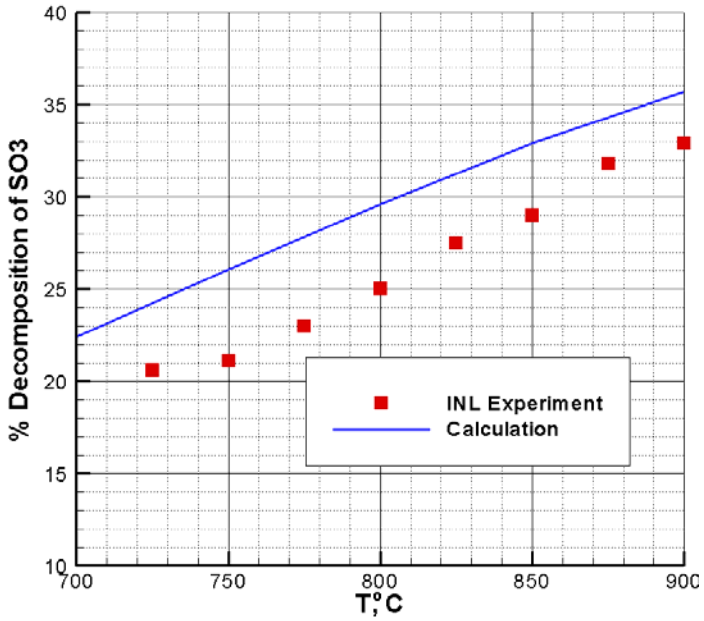

Figure 1. Sulfur trioxide decomposition using 0.1% Pt/TiO_2 as a catalyst.

Stress Analysis and Optimization of Ceramatec HTHX

The finite element calculations of the "Ball on Three Ball Test" for ceramic material for the purpose of selecting the appropriate specimen thickness for future experimental testing was performed for plate thicknesses ranging from 2 to 8 mm. The obtained stresses were compared with different analytical solutions from the literature. The results of the comparisons showed that calculated stresses for the whole range of plates (2 – 8 mm) have good correlation with analytical solutions (see Figure 2).

A finite element model of the "Ball on Three Ball Test" with a disc having micro-channels was studied. The effects of the micro-channel orientation with respect to the supporting balls were investigated. Results of the investigations show that the maximum normal stress does not change significantly after rotating the disc with micro-channels by 60 degrees.

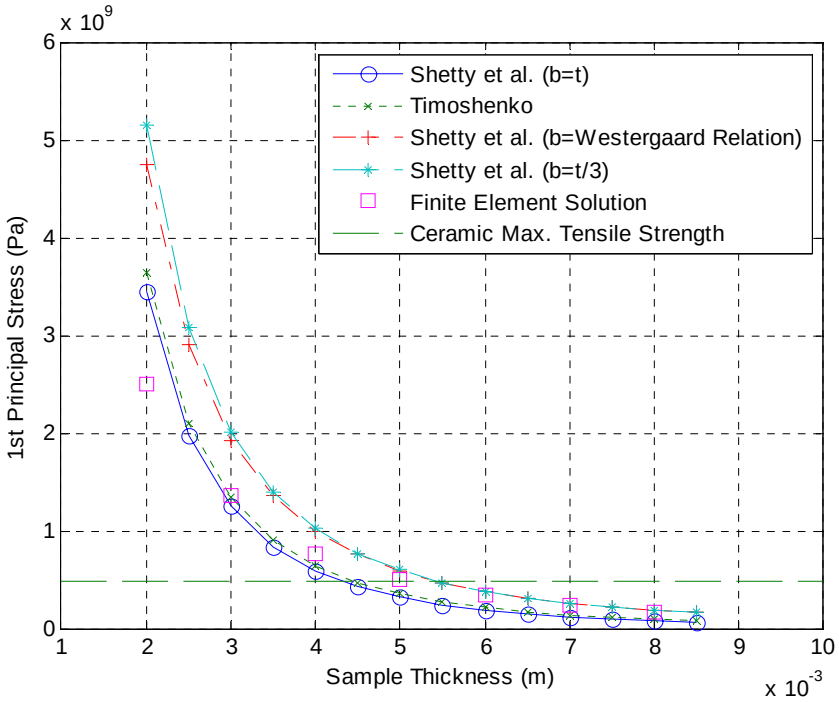

Figure 2. Comparison of the finite element calculations with analytical solutions.

The calculated stresses were also compared with previously calculated stresses for the same plate geometry without micro-channels. The results of the comparison show that the stresses for the plates with micro-channels are larger than those for the case without micro-channels for the whole range of plate thicknesses (2 – 8 mm). The difference of maximal stress between the cases with micro-channels and without micro-channels increased as the plate thickness decreased. The maximum difference is 93% for the 2 mm plate thickness.

Numerical analysis of bayonet HTHX and decomposer based on SNL design

A two-dimensional axisymmetric model of the bayonet heat exchanger and decomposer design of Sandia National Laboratory was developed. The model includes a porous media approach for the pebble bed zone in the decomposer. The surface chemical reaction (SO_3=SO_2+0.5O_2) model was incorporated in the porous media part of the decomposer. Figure 3 shows the decomposer geometry and dimensions. Calculations of flow, heat transfer and chemical reactions in the porous zone decomposer, not the whole SID (Silicon Carbide Integrated Decomposer), were completed. The obtained sulfur trioxide decomposition rate is in the same range as in experiments completed in SNL, but for more precise comparisons some additional information about temperatures, catalyst properties and dimensions of chemical reaction zone used in the SNL experiments are needed.

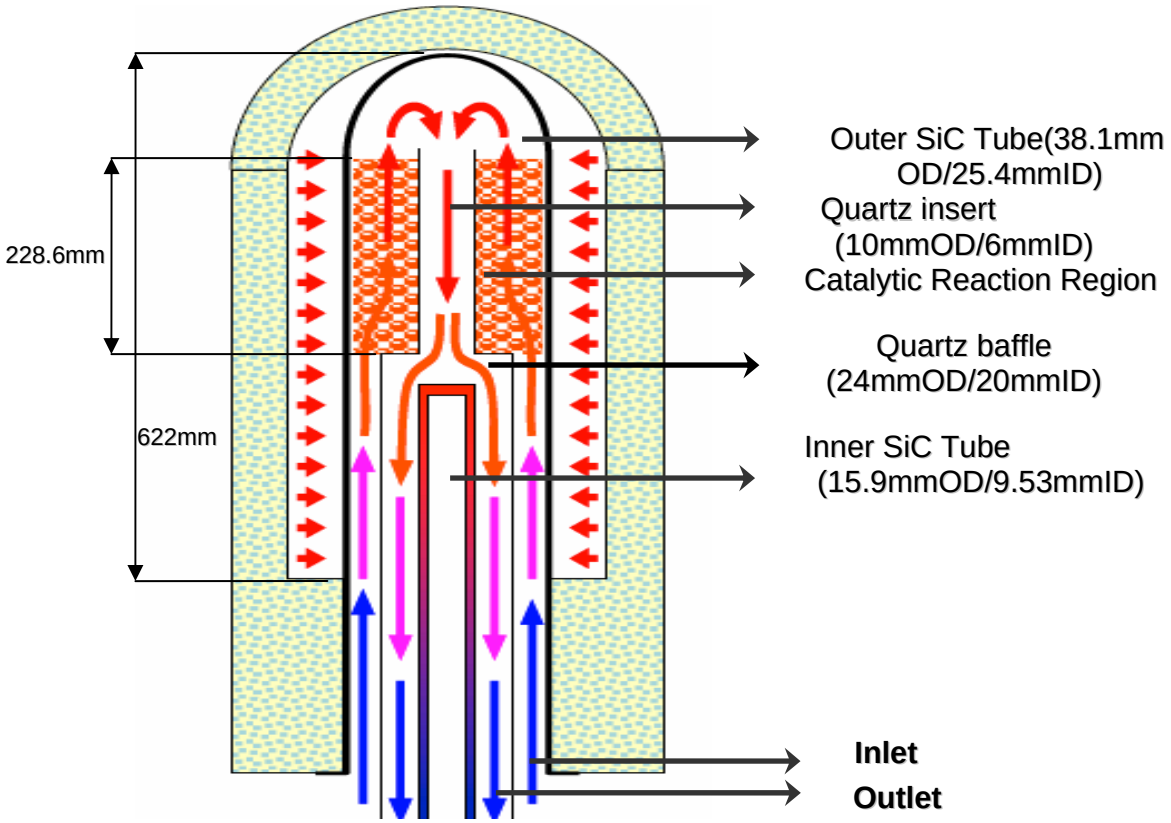

Figure 3. Geometry and dimensions of bayonet high temperature heat exchanger and decomposer.

Numerical analysis of shell and tube HTHX and decomposer

A two-dimensional numerical model using the axisymmetric geometry of shell-and-tube type heat exchanger and decomposer was studied. First, an inside tube was studied in order to understand the catalytic reaction properly in the packed bed region. The computational mesh was created using the Gambit software. The computational domain was created with 3 zones: a preheating zone, a packed bed zone, and an outlet zone. The porous media approach for the packed bed zone was made. Based on a literature review, the porous media properties (i.e., porosity, viscous resistance and inertial resistance) were calculated. Sulfur trioxide decomposition reaction was added to the computation model of the decomposer.

A mesh independence study for the flow with a porous media zone was completed. Based on the study, the computation mesh parameters were chosen (2992 nodes, 2800 cells).

Calculations of flow, heat transfer and chemical reaction for the decomposer were completed. The pressure, velocity and temperature distributions with chemical reaction inside the tube for Reynolds number equal 600 are shown in Figures 4 and 5. According to the calculations, the maximum pressure drop takes place in the porous zone (see Figure 4). The porous zone has high thermal conductivity, therefore the fluid flow temperature becomes equal to wall temperature at the entrance to the porous zone (see Figure 5). The velocity magnitude becomes uniform in the porous zone (see Figure 6).

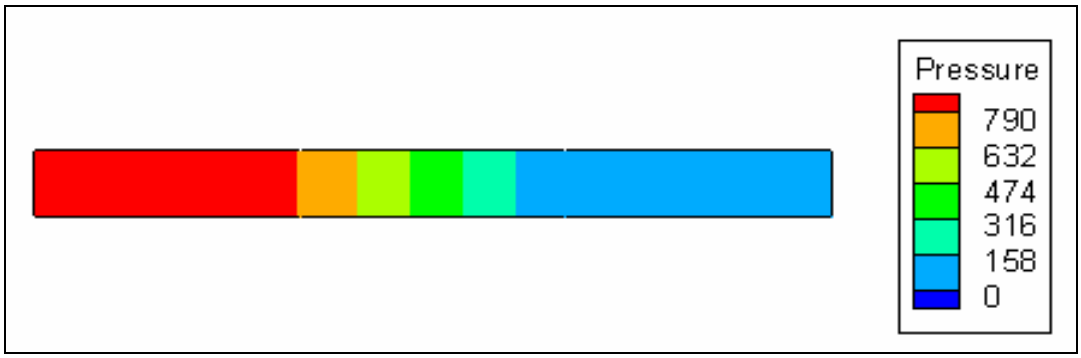

Figure 4. Static pressure distribution for tube and shell HTHX and decomposer (Re=600), Pa.

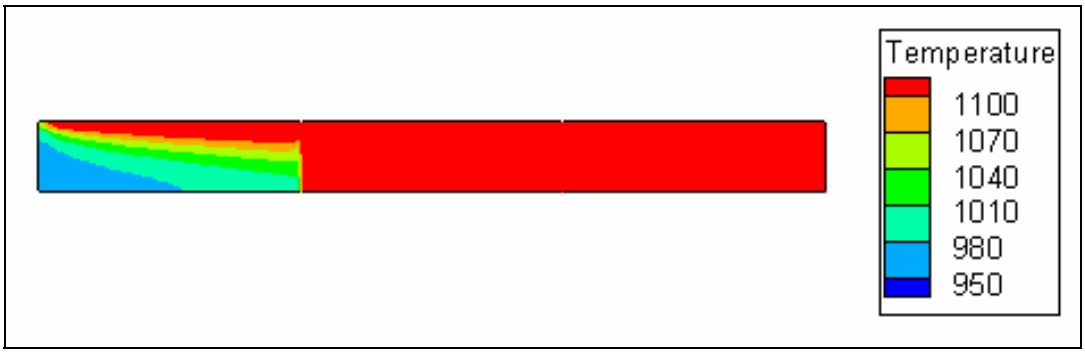

Figure 5. Temperature distribution for tube and shell HTHX and decomposer (Re=600), K.

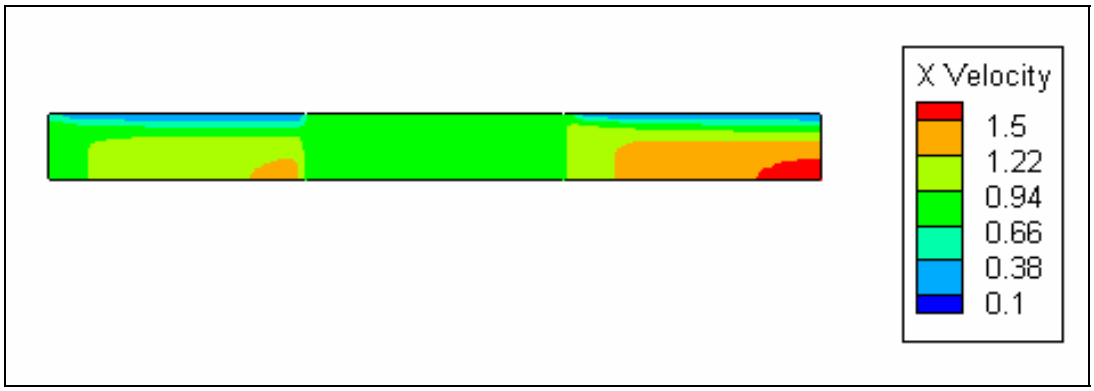

Figure 6. Axial velocity distribution for tube and shell HTHX and decomposer (Re=600), m/s.

Parametric study of the reacting flow for different Reynolds numbers was accomplished (see Figure 7). According to the study the sulfuric acid, decomposition rate decreases with increasing Reynolds number.

The boundary conditions for the bayonet decomposer are listed below:

Porosity - 0.49
Inlet temperature - 873 K
Wall temperature - 1173 K
Operation pressure - 1 atm

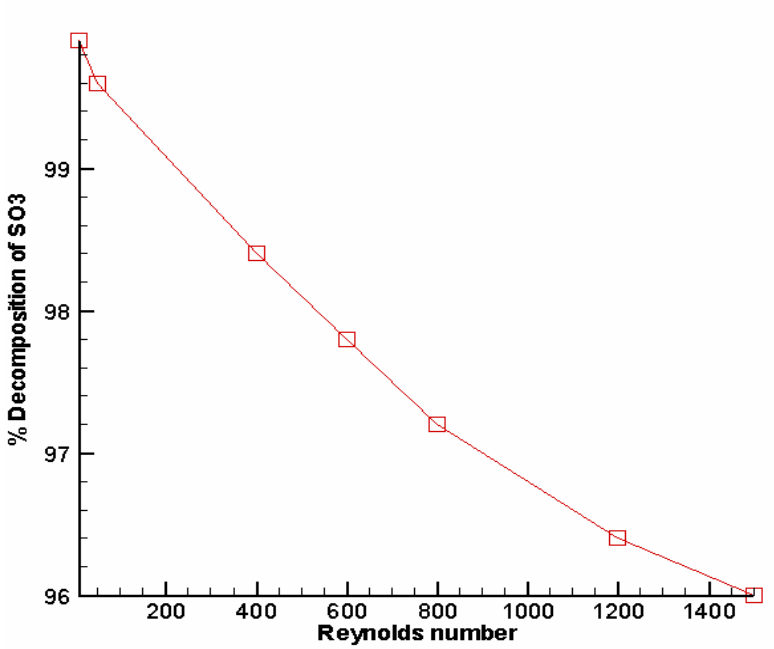

Figure 7. Decomposition percentage of SO_3 for tube and shell HTHX and decomposer with different Reynolds numbers.

1.2 Scaled HTHX Tests (PI: Samir Moujaes, UNLV)

A single-chamber air test section of a 3:1 ratio was built for the hydrodynamic and thermal tests for the off-set strip-fin type heat exchanger. Two electric heating pads were placed on both side of the fin area. The heating power was controlled and varied by the controllers. The test section was insulated by two inches thick fiberglass to minimize the heat loss.

The hydrodynamic tests were run under the isothermal and heated conditions. The friction factors were calculated according to Compact Heat Exchanger (by Kays and London) with periodic-flow-type simplification. It is assumed that a 5% error with a 1% accuracy gas flow meter. The accuracy of the pressure transducer is 0.25%.

The experiments were performed with a Reynolds numbers range from 1800 to 2500 to simulate the prototype heat exchanger flow (see Figure 8). The Reynolds number has an uncertainty of 7%, and the friction factor has an uncertainty of 8%. The pressure data matches for all the cases (double-side-heating, single-side-heating, and no-heating).

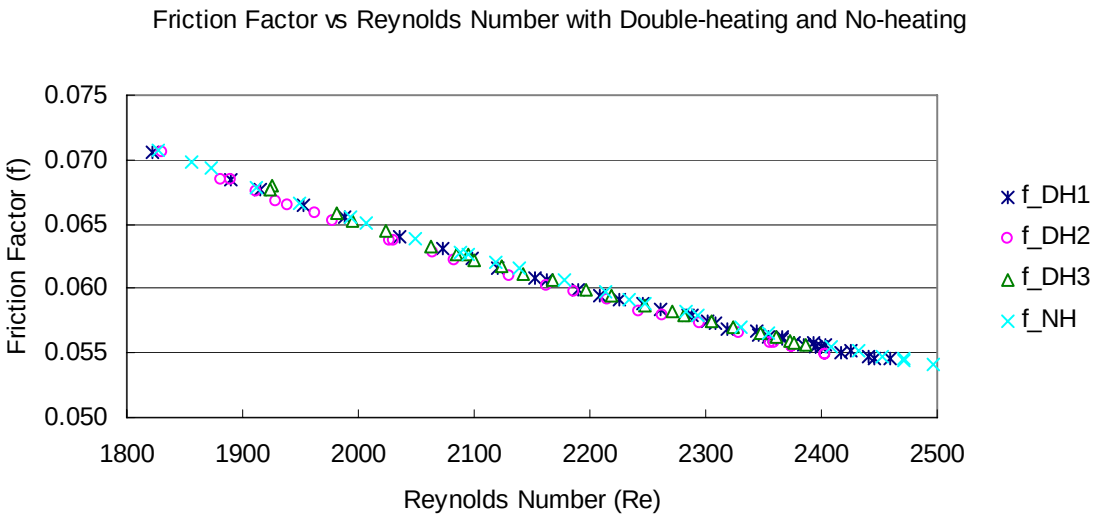

Figure 8. Friction Factor versus Reynolds Number with double-sided heating and no heating.

The thermal experiments were performed for the air single-chamber test section with double-side- or single-side-heating (top or bottom only) at the fin area. The heating power was varied from 50 to 100 W. The average heat loss from the test section is around 40%. The thermocouples generated 4% error, the flowrates had 5% error, and the determination of the heat transfer area had 3% error. The overall heat transfer coefficient has an uncertainty of 8%. The Nusselt number has an uncertainty of 9%.

Because of the high conductivity of the Alloy 6061 in the construction material, the Nusselt numbers for single-side-heating tests are 10% less than that of the double-side-heating tests.

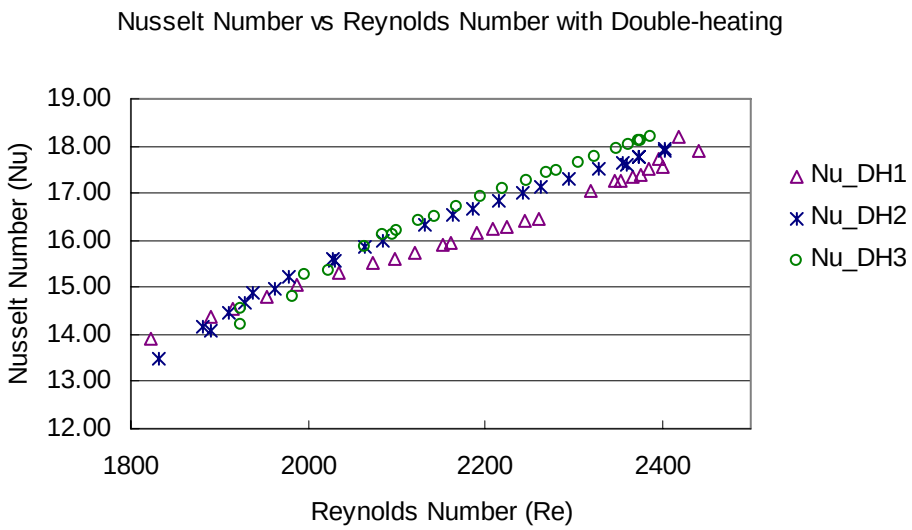

Figure 9. Nusselt Number versus Reynolds Number with double-sided heating.

2.0 UNLV Materials Selection and Characterization (PI: Ajit Roy, UNLV)

2.1 Highlights

- Extensive metallurgical characterization of austenitic Alloy C-276 was performed. Since Alloy C-276 exhibited a unique phenomenon of dynamic-strain-ageing within a specific temperature regime, significant effort was made to develop a basic understanding of this phenomenon.
- Tensile testing of Alloys 617 and 718 was completed. However, the analysis of the resultant tensile data is yet to be performed.

2.2 Technical Summary

The magnitude of failure strain (e_f) for Alloy C-276, was gradually reduced within a temperature range of ambient to 300°C. Such reduction in e_f is attributed to a well-known metallurgical phenomenon of dynamic-strain-ageing (DSA) resulting from the diffusion of solute elements into the metal lattice. The diffusion of these solute elements can impede the dislocation movement from one grain to other, thus reducing the plastic strain.

Transmission electron microscopy was used to characterize dislocations using the resultant micrographs and superimposition of grids onto them (Figure 10). The results indicate that the magnitude of dislocation density (ρ) was highest at temperatures in the vicinity of 200 and 300°C (Figure 11), where reduced plastic strains were noted. The magnitude of ρ was relatively lower at 450°C due to enhanced dislocation mobility and ease of plastic deformation.

The SEM micrographs of Alloy C-276 revealed dimpled microstructures in tensile testing at temperatures up to 600 °C, indicating ductile failures. However, brittle failures were seen at temperatures of 700 and 800°C, as illustrated (Figure 12).

Since the phenomenon of DSA is influenced by both temperature and strain rate, the effects of both these parameters on the activation energy were studied. An average Q value of 55 kJ/mole was calculated based on these analyses.

A non-linear relationship was noted in the log true stress (σ) vs. log true strain (ε) plot according to the Hollomon equation. Therefore, the Ludwigson approach was applied to determine the magnitude of n that ranged between 0.68 and 0.75 for specimens tested at 200, 300, 400 and 450°C. The relationships between log σ and log ε using both approaches are illustrated (Figure 13).

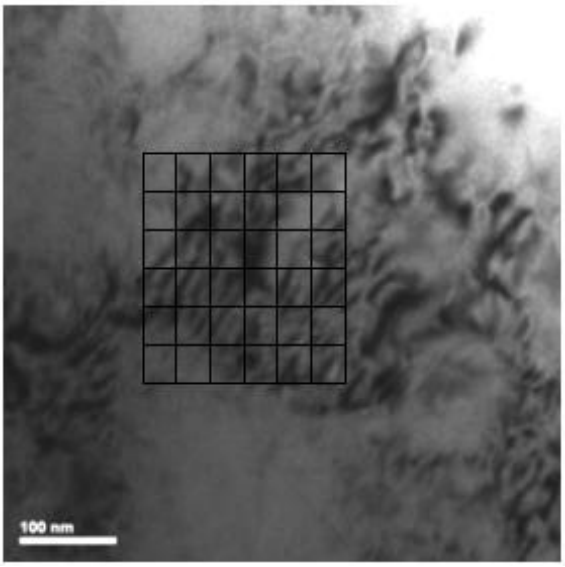

Figure 10. Calculation of ρ by Line Intersection Method.

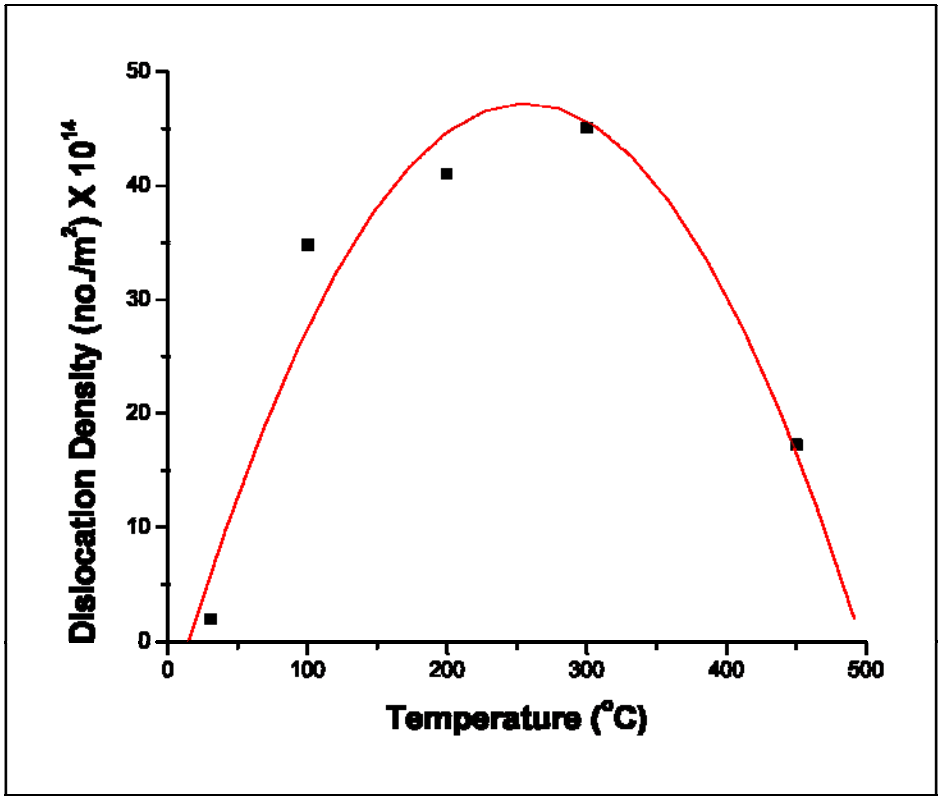

Figure 11. Dislocation Density vs. Temperature.

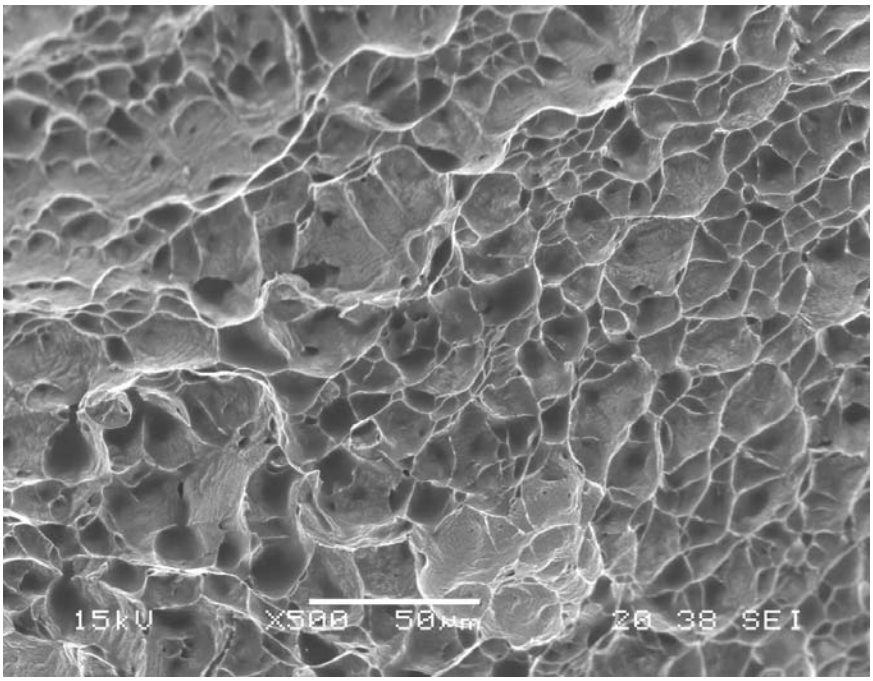

(a) 600°C

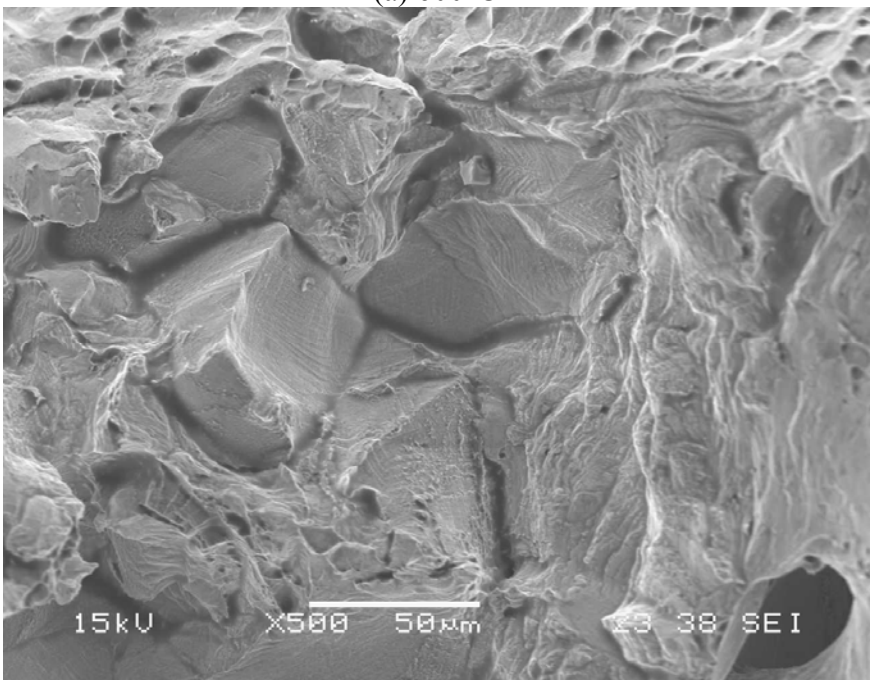

(b) 700°C

Figure 12. SEM Micrographs of Alloy C-276, 500X

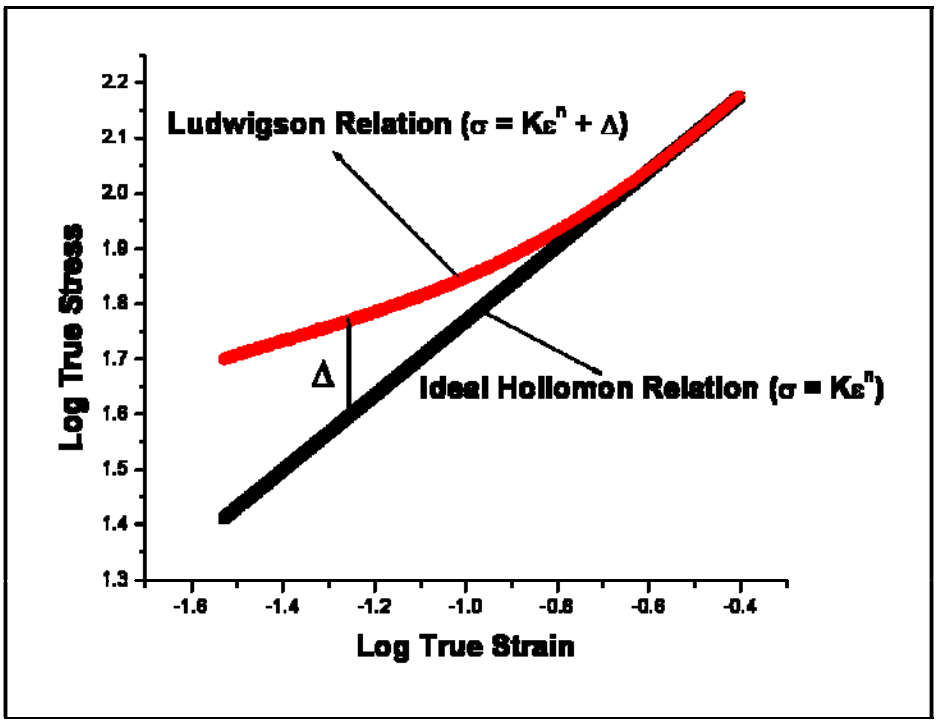

Figure 13. Hollomon and Ludwigson Relation Plots.

The susceptibility of Alloy C-276 to stress corrosion cracking (SCC) in room temperature acidic solution (PH~1) was determined by using precracked and wedge-loaded double-cantilever-beam (DCB) specimens. Measurable crack extension and reduced stress intensity factor values were observed upon completion of 30 days tests. An SEM micrograph showing regions of fatigue precrack, SCC and fast fracture is illustrated (Figure 14).

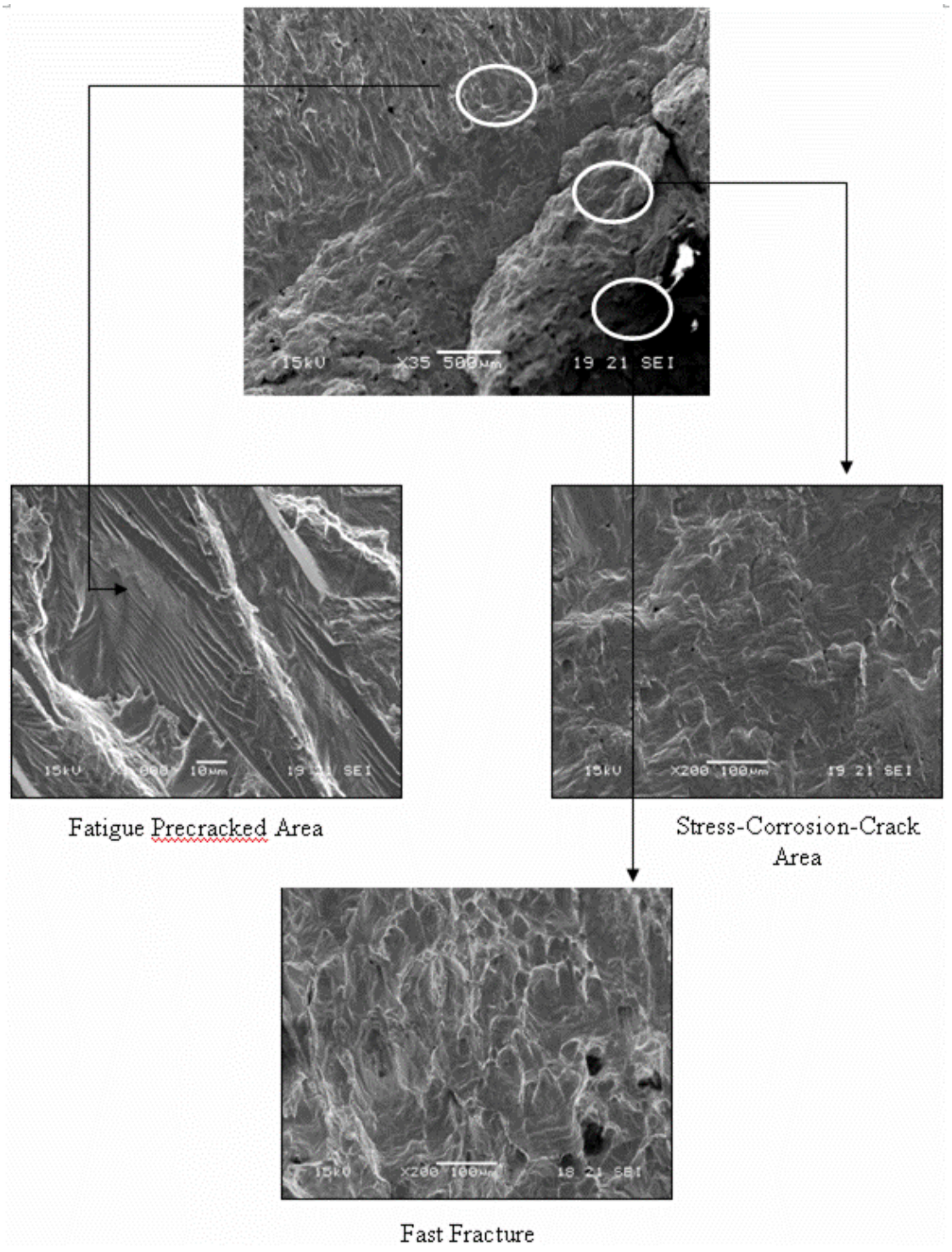

Figure 14. SEM Micrographs showing Fractures at Different Regions of DCB Specimens.

The results of tensile testing involving Alloy 617 are illustrated (Figure 15), showing superimposed engineering stress-strain (s-e) diagrams as a function of the testing temperature. The analysis of tensile data is in progress.

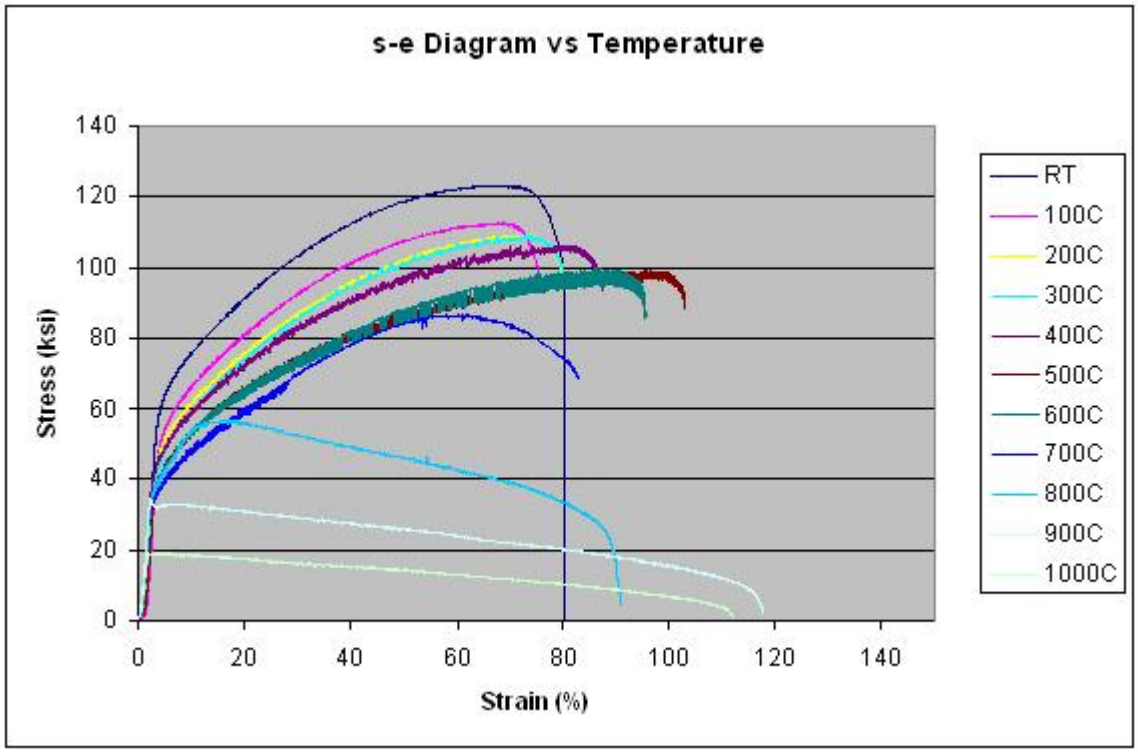

Figure 15. Superimposed stress-strain diagrams for Alloy 617.

3.0 Materials, Design and Modeling for C/SiC Ceramic Heat Exchangers, (PI: Per Peterson, UCB)

3.1 Highlights

- The design of the next ceramic SiC/C heat exchanger was completed and was sent to the vendor COI for fabrication using the PIP method. This task is focused on process optimization, particularly in the area of plate lamination methods. The new heat exchanger geometry has a counter-flow configuration, and is designed so that it can be used to test CVD coating of pyrolytic carbon on the interior surfaces of the flow channels, to provide a corrosion resistant coating for liquid fluoride salts.
- Further work was performed to develop global thermal and stress modeling methods for compact heat exchangers, based on the porous media approximation. This includes better approaches to estimate the effective porous media properties based on data obtained from unit-cell calculations.
- Researcher Dr. Jens Schmidt from the German Aerospace Center (DLR) completed a 3-month visit at Berkeley, to collaborate on the design of liquid-silicon infiltrated ceramics for application in the S-I hydrogen production process.

3.2 Technical Summary

PIP C-C/Si-C Composite and Other Composite Materials Study

The subcontract to COI for a previous task was completed, and the fabrication of a prototype cross-flow heat exchanger using the PIP method was achieved (Figure 16). Experience from the fabrication of this test heat exchanger will be used in the development of a new set of Teflon molds for a heat exchanger to be built under a new task this spring. This effort will focus on further process optimization to reduce residual porosity and to improve lamination methods, and will fabricate a heat exchanger test article with a closed flow path that can be used to demonstrate CVD SiC and pyrolitic carbon coating of interior heat exchanger flow channels. Figure 17 shows the heat exchanger flow channel design that will be used.

Figure 16. PIP test plate stack fabricated last quarter.

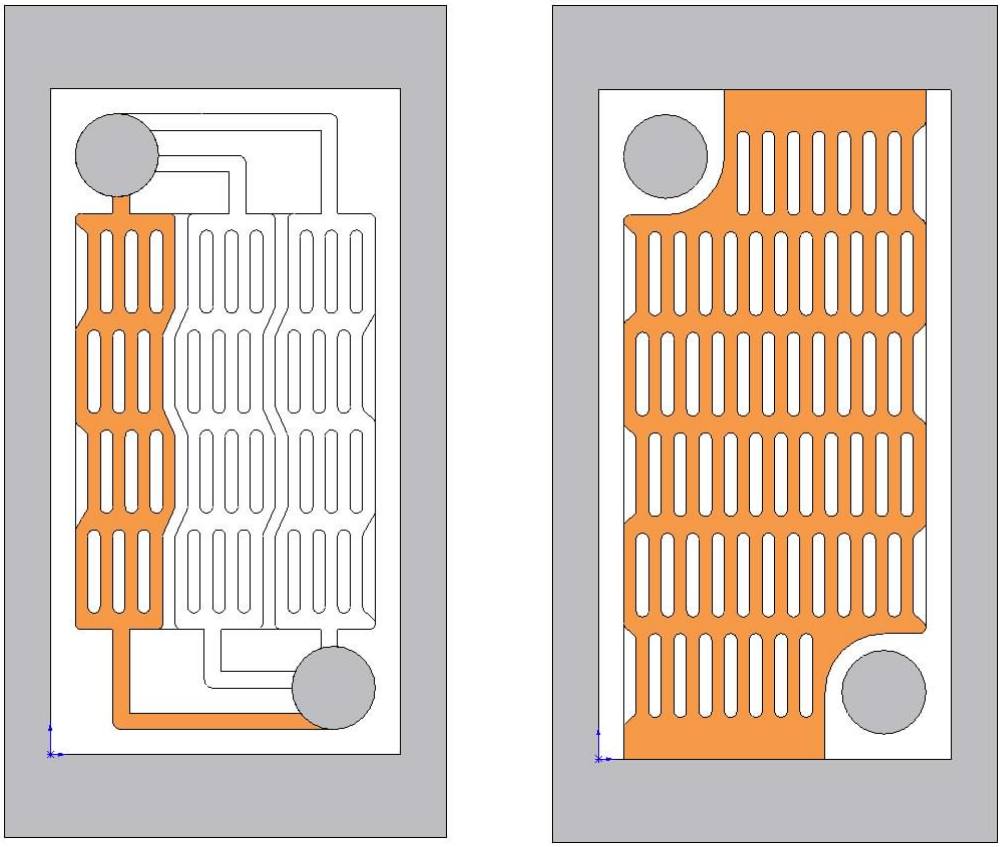

Liquid salt flow channels Helium flow channel

Figure 17. Flow channel design developed for next COI heat exchanger.

Dr. Jens Schmidt, from the German Aerospace Center (DLR), visited the University of California, Berkeley for a 3-month research sabbatical from September 29 to December 27, 2006. This visit involved collaboration on high-temperature ceramics for application to the thermo-chemical production of hydrogen. A detailed technical survey was performed to improve the current understanding of potential applications for liquid silicon infiltrated (LSI) composites for use in the sulfur-iodine process for hydrogen production.

Currently, most work in thermo-chemical hydrogen production methods focus on methods that rely on the high temperature thermal decomposition of sulfuric acid into SO_2 and oxygen, and lower temperature reactions or electrolysis with water to produce hydrogen and regenerate sulfuric acid. Silicon carbide, with small amounts of residual silicon, were demonstrated by Sandia National Laboratory to be an effective material for the decomposition reaction, as well as other chemical process steps in the S-I process, giving the flexibility of LSI manufacturing methods a potentially important advantage.

Dr. Schmidt's work involved an extensive investigation and review of S-I process technology, and included visits and presentations at General Atomics in San Diego, California, Sandia National Laboratory in Albuquerque, New Mexico, and the University of Nevada, Las Vegas.

Dr. Schmidt documented his work in an extensive and excellent report, which will provide the basis for ongoing collaboration in this area. Near term work will include compatibility studies for LSI composites with S-I process fluids and with high-temperature liquid fluoride salts that may be used as heat transfer fluids, and investigations of fabrication methods for LSI heat exchangers using wood-based materials developed at DLR. Figure 18 shows recent progress at DLR in developing methods for low-cost molding of perform materials for fabrication of LSI heat transfer equipment.

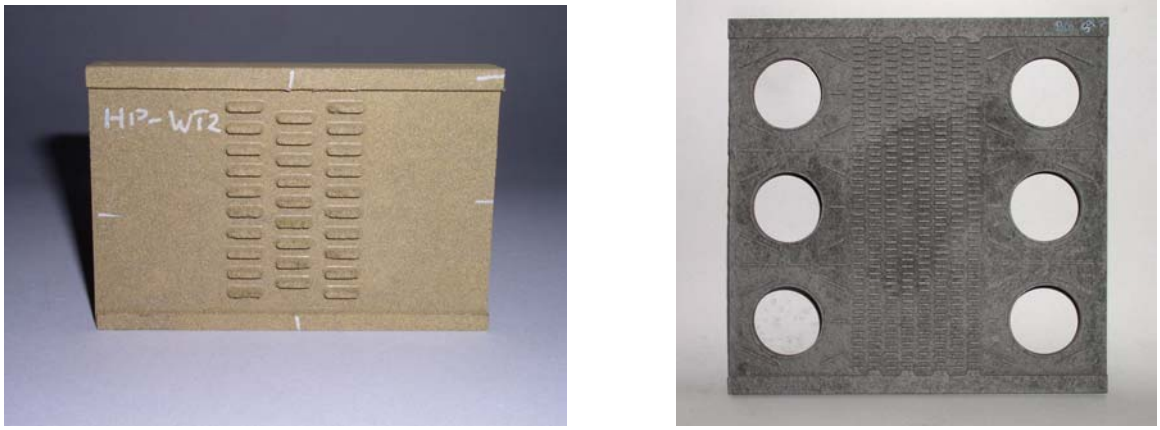

Figure 18. DLR prototype wood composite test plate (left, 80x120 mm²) with fins (length~ 10 mm). DLR prototype HX plate (~ 300x300 mm²) in OSF design made from carbon bulk material with high expense in machining. Dimension of fins: 4 mm in height, 2 mm in width, and 10 mm in length (right).

Continuing work in the area of ceramic heat exchangers will shift in focus toward design, analysis and experiments for liquid salt compatibility. This will include work to apply CVD pyrolytic carbon coatings to SiC composite samples for liquid salt corrosion testing, and further analytical work on corrosion and safety issues for liquid salt intermediate loops. A detailed report on previous UC Berkeley work in this area was also released.

Compact heat exchanger thermal/mechanical design study

UC Berkeley continued work to develop a global thermal and fluid mechanics model for compact ceramic and metal heat exchangers based on the porous media approximation. This approximation is valid when the flow structures in the heat exchanger are small compared to the overall heat exchanger size, and when these flow structures are repeated in such a way that they can be represented as repeating unit cells. Offset strip fin heat exchangers, and Heatric type heat exchangers.

Further work will continue in this area in the spring.

4.0 Corrosion Studies of Candidate Structural Materials in HI_x Environment as Functions of Metallurgical Variables (PI: Bunsen Wong, General Atomics)

4.1 Immersion Testing of Materials in HI_x-H_3PO_4 (Iodine Separation)

Testing in the iodine separation system with circulating acid is continued this quarter. The goal was to test qualified materials in a non-static environment in order to identify any modification in their corrosion behavior. Figure 19 shows a section of Ta-2.5W tube that was jointed together with a Ta weld. It was immersion tested in a H_3PO_4 – HI_x circulating bath. After 178 h of testing, there is no sign of corrosion. Testing is continuing with this and other similar components in the circulating acid test system.

Testing of coupons and parts that were coated with a Ta layer in the iodine separation environment began. Two different methods were used to coat the stainless coupons and part. First, parts and components were electroplated with a layer of Ta. In the other approach, specimens were coated with a sputtered Ta film. In some of the sputtered specimens, the Ta film is anodized. These coated specimens were tested in both the static and flow environment.

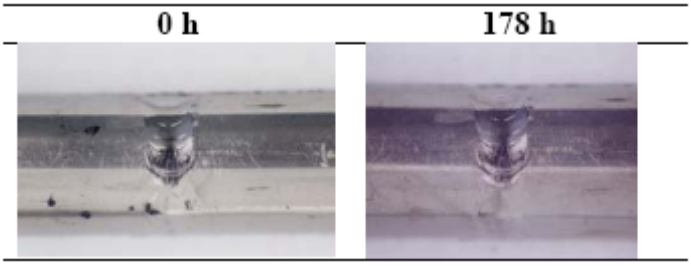

Figure 19. A Ta-10W tube section with a Ta weld that was tested in the H_3PO_4 and HI_x circulating bath.

Swagelok components (fittings, tubing and ferrules) plated with Ta were tested in the circulating H_3PO_4 – HI_x bath. These components are critical in the construction of a shell and tube heat exchanger. Figure 20 shows a T-joint that was tested. The body of the joint itself does not show any sign of corrosion whereas on the threads, the acid has attacked the stainless based material underneath the Ta-layer. This is caused by mechanical damage to the Ta layer which led to the stainless beneath being exposed. A number of ferrules have also been tested in the circulating bath. Figure 21 shows the pretest examination of a ferrule that was swaged onto a Ta-10W tube. It shows mechanical damage to the Ta layer that was plated on the back ferrule. As expected, the acid attacked the stainless under the damaged Ta layer (Figure 22). In the actual set up, these two areas (i.e., the plated threads and the back ferrule) will not be exposed to any test fluids. However, in light of these findings, work procedures were established to avoid similar damage.

Figure 20. A stainless T joint plated with Ta that was tested in the H3PO4 and HIx circulating bath for 114 h. Corrosion was observed in the threads.

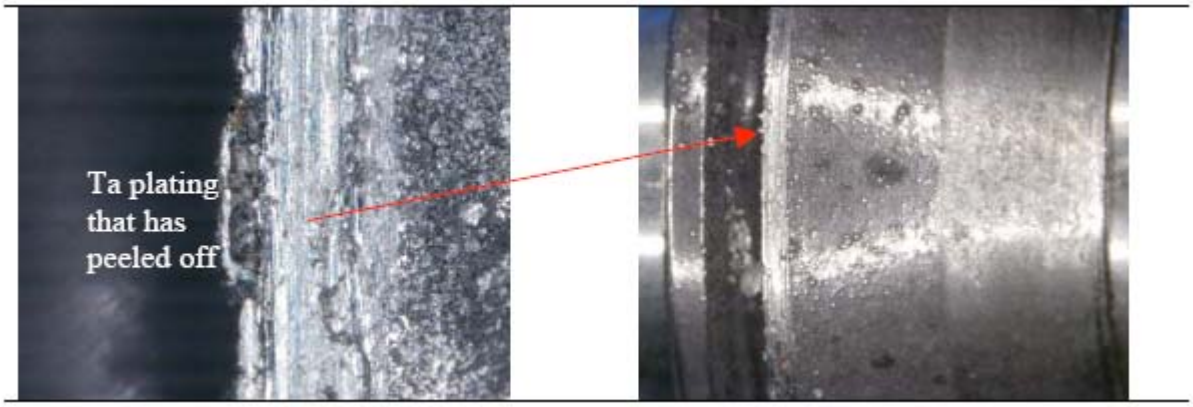

Figure 21. Pretest examination of a ferrule that was swaged onto a Ta-10W tube.

Figure 22. A ferrule that was swaged onto a Ta-10W tube and was tested in the H_3PO_4 and HI_x circulating bath for 71 h. Corrosion can be seen in areas where the protecting Ta has previously been damaged.

At the front of the ferrule, contact with the flowing acid is expected. Examination of all the tested ferrules did not show any sign of corrosion and the Ta layer is intact. An example is show in Figure 23. Hence, the Ta plating works satisfactory so far but testing under different working conditions is needed.

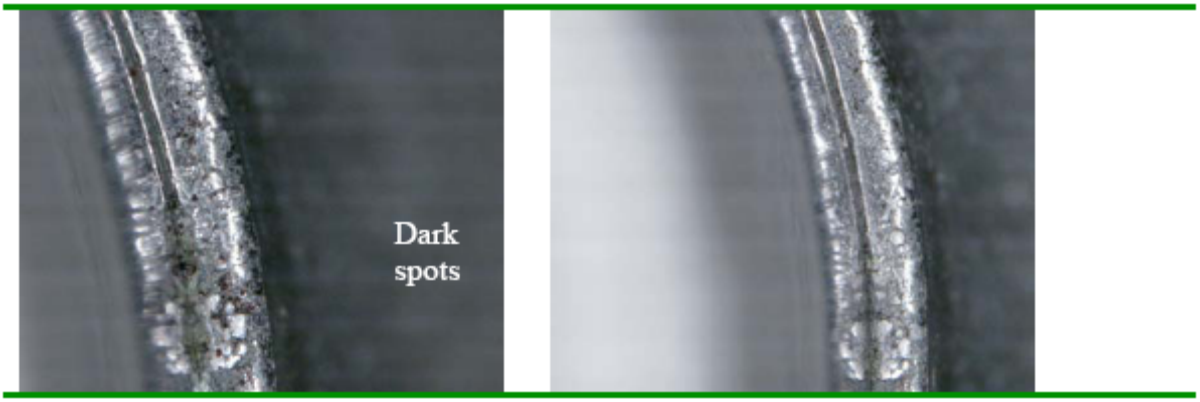

Figure 23. An example of the front of a ferule that has undergone testing in the $H_3PO_4 – HI_x$ circulating bath. There is no sign of corrosion. Dark spot at the front short edge of the ferrule are not corrosion related as they can be easily removal with a Q-tip.

Figures 24 and 25 show two Cr-Mo steel coupons that were tested in a static iodine separation environment. They were coated with sputtered Ta and anodized sputtered Ta. The coupons were severely corroded and it is because the Ta layer on top is probably too thin and pinholes exist in the film. Hence, the acid was able to attack the stainless material through these pinholes.

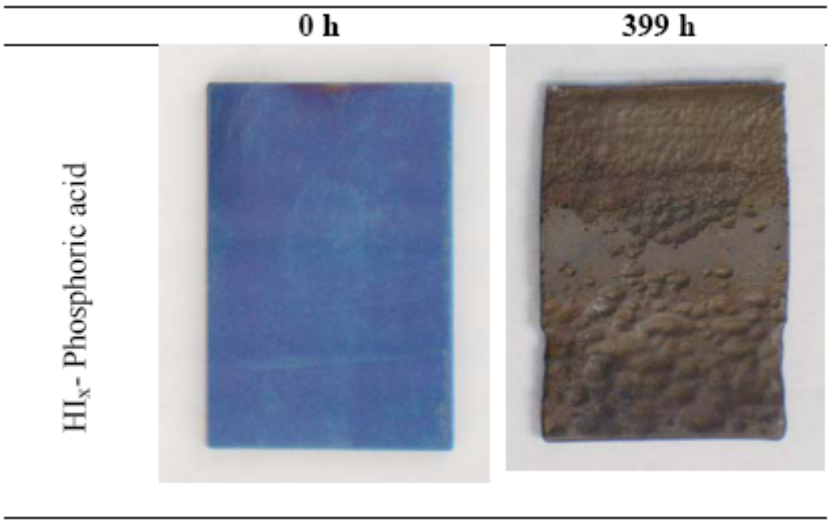

Figure 24. A Cr-Mo steel coupon coated with sputtered Ta and then anodized. Severe corrosion took place after immersion in HI_x-H_3PO_4 acid mixture at 140°C for 399 h.

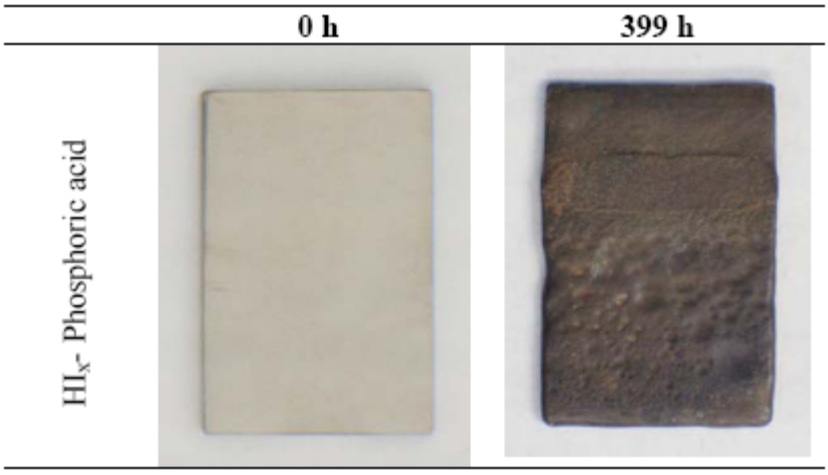

Figure 25. A Cr-Mo steel coupon coated with sputtered Ta. Severe corrosion took place after immersion in HI_x-H_3PO_4 acid mixture at 140°C for 399 h.

4.2 Immersion Testing of Materials in boiling H_3PO_4 (Concentrated H_3PO_4)

The testing of heat exchanger candidate materials in concentrated H_3PO_4 is ongoing. The emphasis is on the effect of chemical contaminants on materials that had shown good corrosion properties in conc. H_3PO_4. Figures 26 and 27 show the effect of HI and HI + I_2 additions on C706 (CuNi). With only the addition of HI, there is little corrosion observed in the C706 coupon (Figure 26). However, severe corrosion can be observed once I_2 is added (Figure 27).

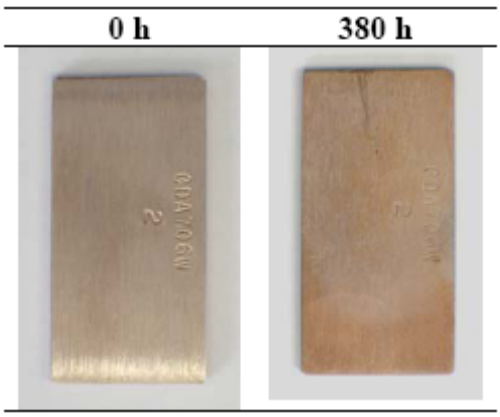

Figure 26. C706 coupon tested in boiling phosphoric acid with HI (92H_3PO_4-3HI-5H_2O wt%). at 250°C for 380 h.

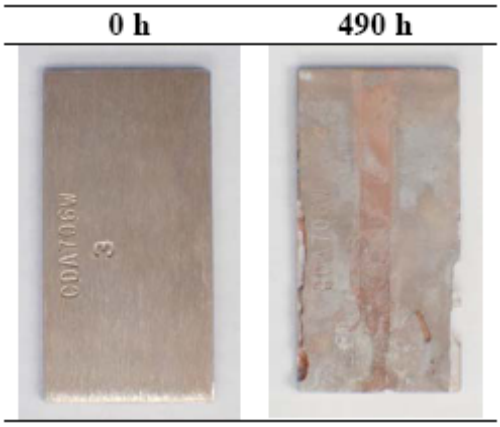

Figure 27. C706 coupon tested in boiling phosphoric acid with HI and I2 (68.8 H_3PO_4-14.4HI-16.1H_2O-0.7I2 wt%) at 190°C for 490 h.

Similarly, the addition of HI and I_2 cause sever corrosion in the Ag coupon. Figure 28. shows an Ag coupon that was tested in an H_3PO_4 + HI + I_2 boiling acid bath. It was severely corroded during test. Hence, both C706 and Ag are not really suitable for this application as varying amount of HI and I_2 are expected in the phosphoric acid circulating in Section III.

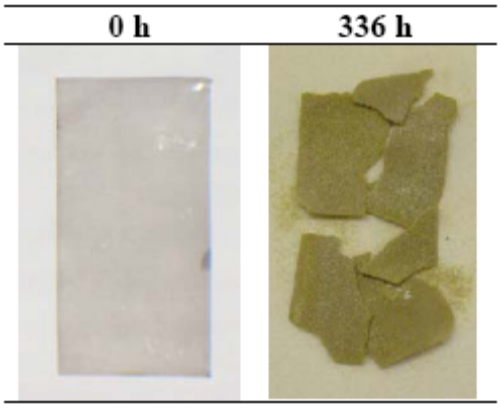

Figure 28. Ag coupon tested in boiling phosphoric acid with HI and I2 (68.8 H_3PO_4-14.4HI-16.1H2O -0.7I2 wt%) at 190°C for 336 h.

Screening with a Ti grade 2 and a Cr-Mo steel coupon with coated with sputtered Ta in boiling conc. H_3PO_4 has also been conducted. Both coupons were severely corroded.

4.3 Testing of Materials in HI + I_2 + H_2 (HI gaseous decomposition)

Long term testing of Hastelloy C-22 and C-276 coupons in both the HI gaseous decomposition and the iodine condenser environments were completed (Figures 29 and 30). No severe corrosion can be observed and the corrosion rate of both materials falls within the acceptable range but not as good as B2 (Table 1).

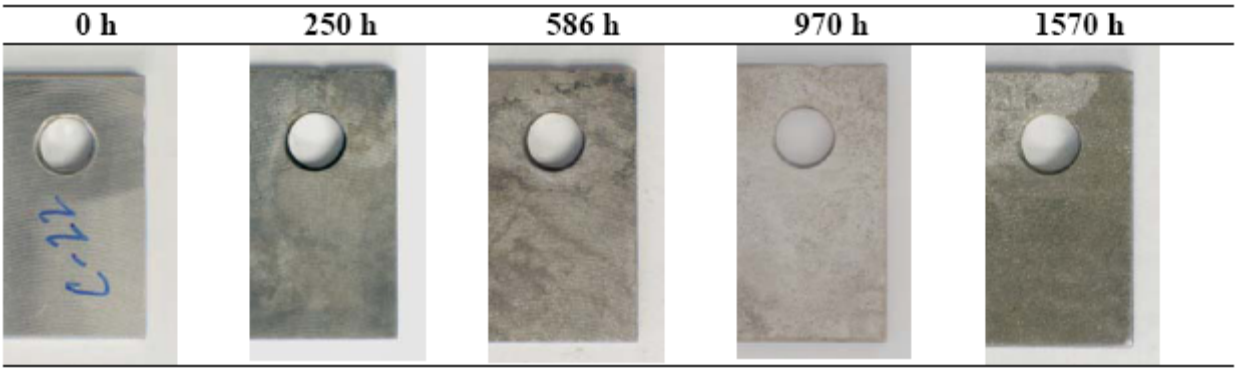

Figure 29. C-22 coupon tested in the gaseous HI decomposition environment for 586 h.

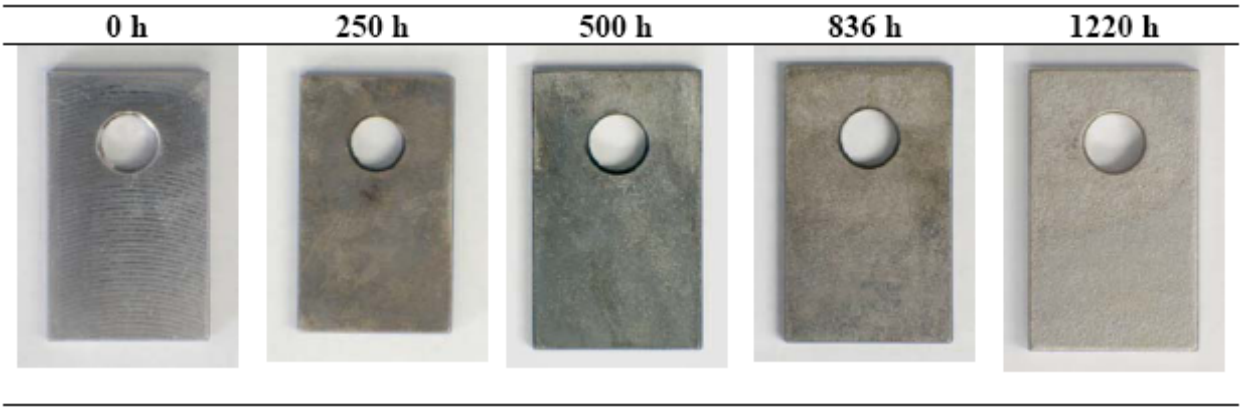

Figure 30. C-276 coupon tested in the gaseous HI decomposition environment for 836 h.

Table 1. Corrosion rate of materials tested in the HI gaseous decomposition (450°C) and iodine condenser environment (160°C) Sample Hours Corr. rate (mpy)

Sample	Hours	Corr. rate (mpy)
B2	1172	2.549
B2*	1172	0.823
C-22	1570	10.699
C-276	1220	13.497
Monel*	1570	0.891

**iodine condenser*

The applicability of Monel in the HI decomposition environment has also been studied. Figures 31 and 32 show the Monel coupons that were tested in the HI reactor and the iodine condenser respectively. The corrosion rate of Monel in the reactor is relatively high (67.8 mpy) so it is not suitable for use it this environment. On the other hand, Monel seems to handle the iodine condensation environment well and the corrosion rate suggests that it can be used for the iodine condenser (Table 1).

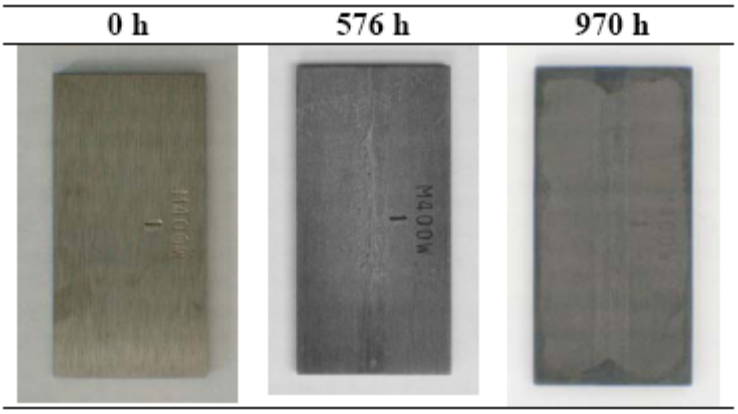

Figure 31. Monel coupon tested in the gaseous HI decomposition environment for 576 h.

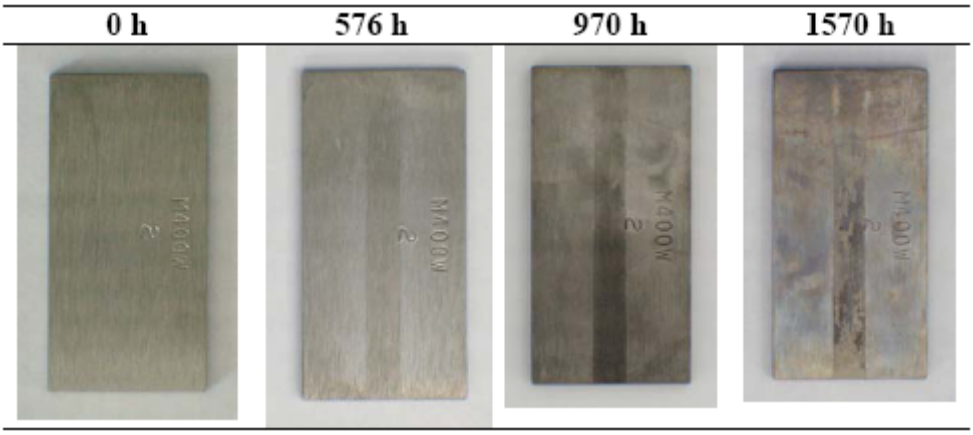

Figure 32. Monel coupon tested in the gaseous iodine condenser environment for 576 h.

Testing of pre-stressed C-ring and U-bend specimens fabricated from Hastelloy C-22 and C-276 in the HI decomposition environment was completed during this quarter. The C-ring specimens were pre-loaded to 98% of materials' yield strength and the U-bend specimens were load to the optimal stress level for comparison between the two materials. Figures 33–36 show the test progression of the Hastelloy C-22 and C-276 C-ring and U-bend specimens. No crack has formed in any of the specimens tested even though they all exhibit minor weight loss (Table 2). This shows that Hastelloy C-22 and C-276 will probably not be susceptible to stress corrosion cracking at the pressure level that will be present within the HI decomposer.

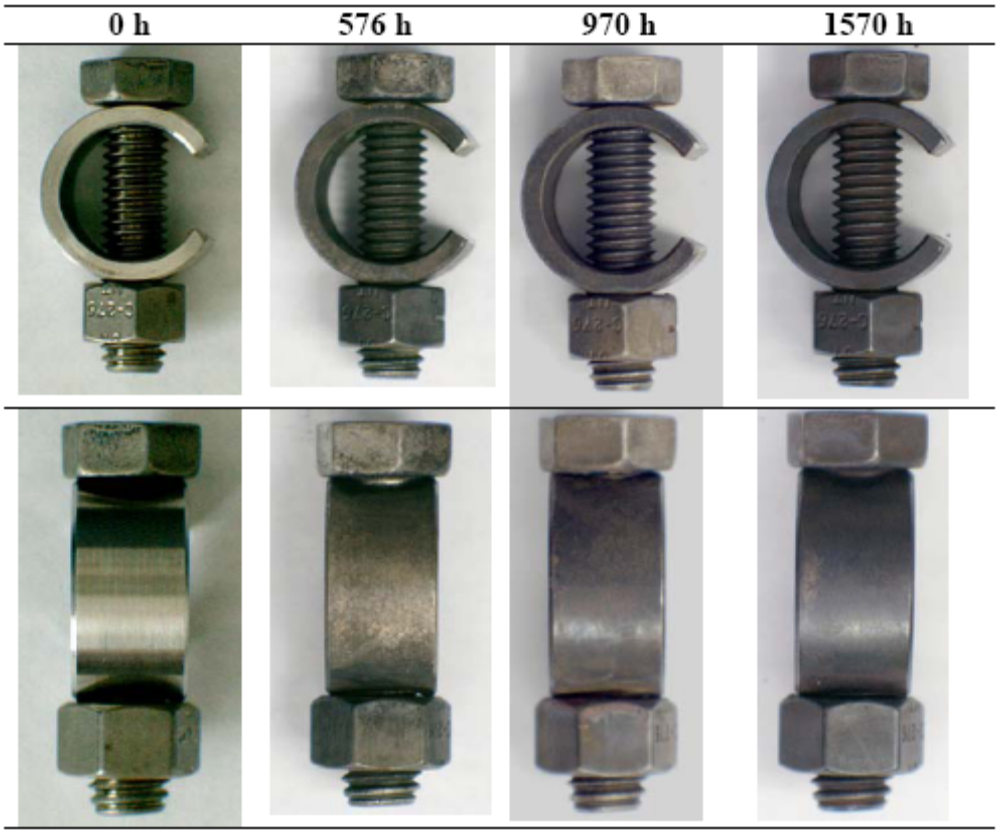

Figure 33. C22 C-ring specimen coupon tested in the gaseous HI gaseous decomposition environment (HI + I_2 + H_2) at 450°C.

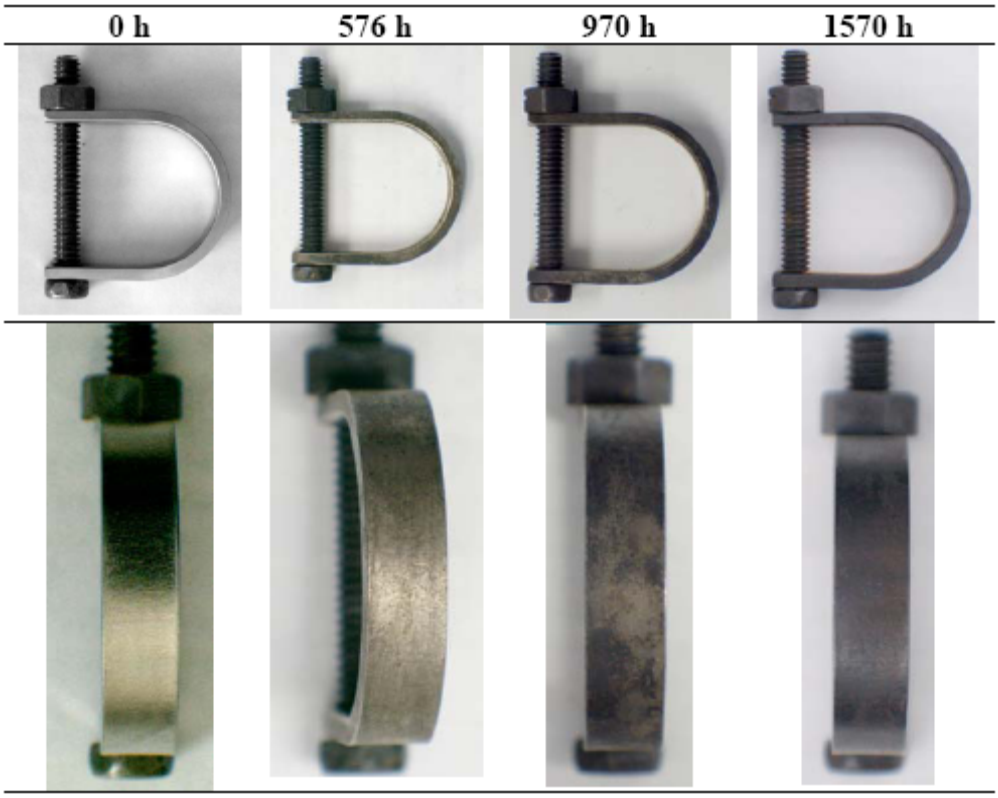

Figure 34. C22 U bend specimen coupon tested in the gaseous HI gaseous decomposition environment (HI + I_2 + H_2) at 450°C.

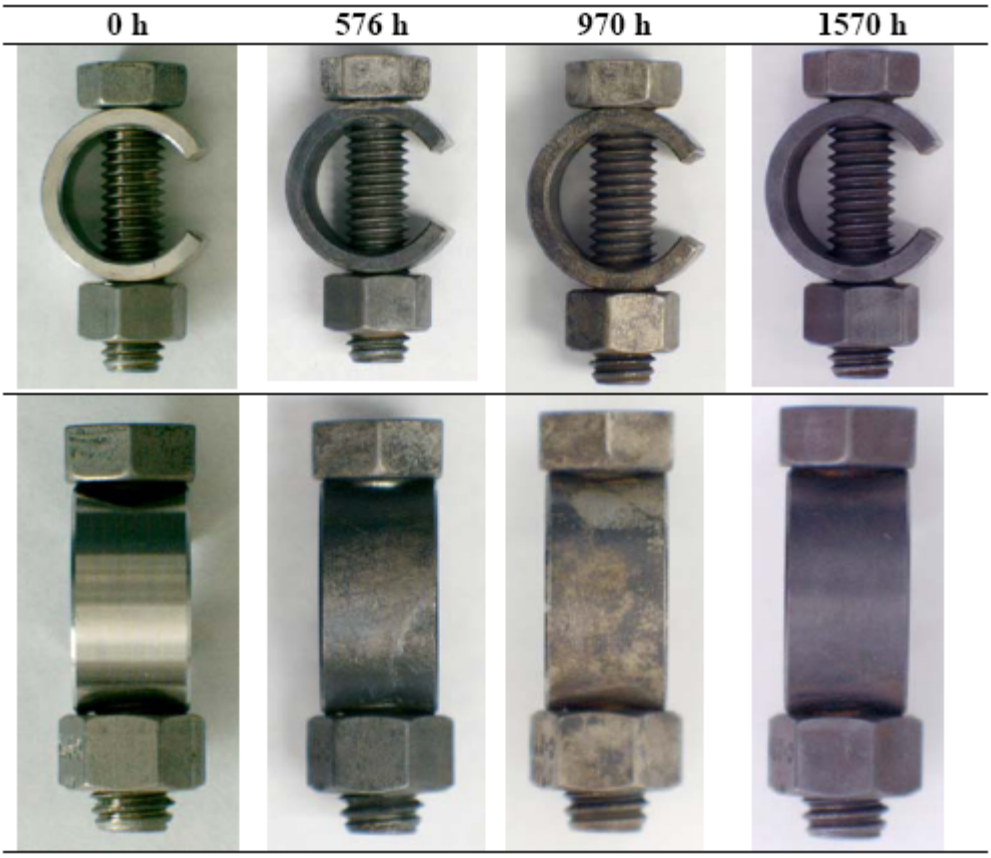

Figure 35. C276 C-ring specimen coupon tested in the gaseous HI gaseous decomposition environment (HI + I_2 + H_2) at 450°C.

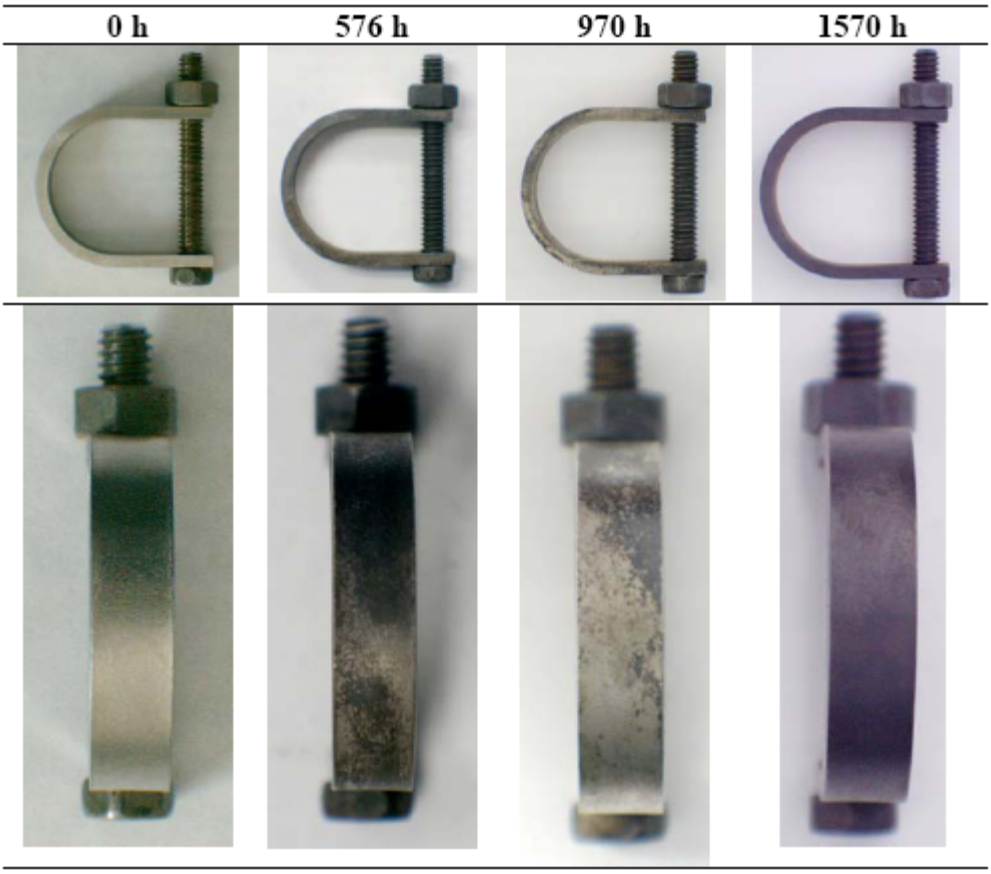

Figure 36. C276 U bend specimen coupon tested in the gaseous HI gaseous decomposition environment (HI + I_2 + H_2) at 450°C.

Table 2. Weight loss of C-22 and C-276 C-ring and U-bend specimens tested in the HI gaseous decomposition environment at 450°C

	Hours Test and Sample weight							
	T1(hr)	W1(g)	T2	W2	T3	W3	T4	Δ W (g)
C-22 C ring	51.305	576	51.080	970	50.889	1570	50.754	-0.551
C-22 U bend	36.911	576	36.644	970	36.431	1570	36.258	-0.653
C-276 C ring	51.332	576	51.089	970	50.855	1570	50.725	-0.607
C-276 U bend	37.661	576	37.345	970	37.069	1570	36.820	-0.841

4.4 Functionality Testing of Valve in Flowing HI_x

The first functionality test of a process component in flowing HI_x was completed. In this case, an air actuated Teflon valve with was cycled (open-close) every 90 s for a total of 1000 cycles with HI_x circulating through it. Figure 37 shows a picture of the valve after testing was completed. There is iodine penetration in the Teflon layer and some sign of corrosion was observed in the housing. This is probably due to the accidental spillage during test set up. Further analysis is being undertaken. The post test valve was pressure tested up to 100 psi.

Figure 37. A Teflon valve that was actuated for 1000 cycles in flowing HI_x at 140°C.

5.0 Chemistry Support Studies (PI: Allen Johnson, UNLV)

There was a large amount of work accomplished in late 2006 organizing and examining the scope of the UNLV efforts in thermochemical hydrogen generation. As part of the chemical characterization work package, a corrosion-resistant modulated molecular beam mass spectrometer-monitored vacuum furnace facility was proposed. This facility is outlined in Figure 38. The system is a modification of a system previously used at UNLV to look at high temperature combustion processes.

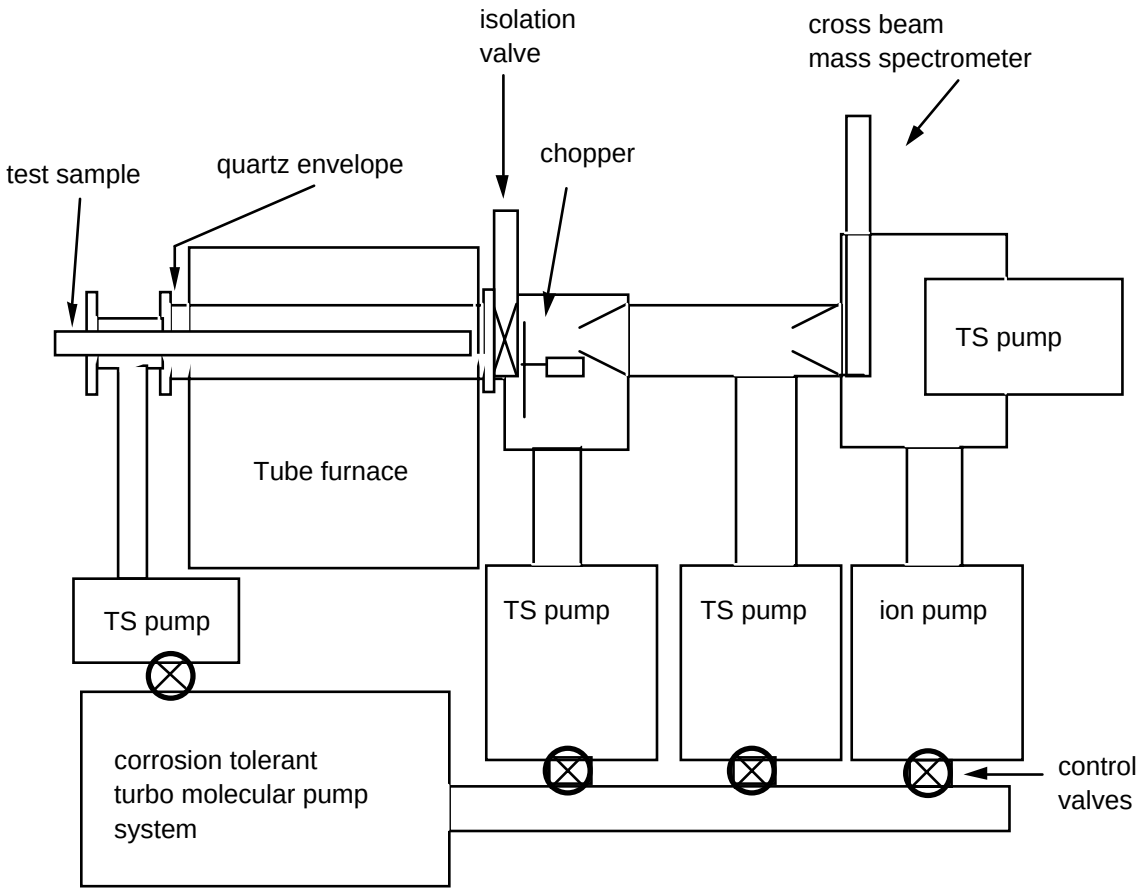

Figure 38. Proposed Chemical Characterization Facility.

The salient modifications were made to the vacuum system to tolerate the acidic and halogen containing compounds common in thermal hydrogen generation chemistries (i.e. the S-I process). Titanium sublimation (TS) pumps and ion pumps have no moving parts, and thus are more resistant to corrosion than other pumps. However, every once in a while it is necessary to pump gasses that ion and TS are not good at, and so a turbo pump was supplied.

This facility will allow a number of materials related studies, measuring permeation and failure with gas pressure loads under chemical and thermal conditions characteristic of the thermal hydrogen generation processes. Further, it can measure the chemical species and intermediates

for process loops interfaced to the facility. We have solicited input from other workers to get access to propose process loops.

Contributions were made to the discussion of molten salt loops. Amongst other things, an arrangement of pumps and heat exchangers were suggested (Figure 39) that address two problems in thermal hydrogen generation plants – pressure matching the primary loop to the process loop, and isolating the loop sections on component failure.

The central realization was that the pressure difference between the loops need not be accommodated in the heat exchanger – in fact one could do it in the pumps. For a molten salt (non-compressible high heat capacity liquid) one sees that a split coolant pumping system, with a pump on either side of the heat exchanger, can isolate the heat exchangers from any pressure drop. A positive displacement pump (piston and valves, a swash plate hydraulic pump/motor, for example) can function as a pump or a motor – if you connect the drive shafts of the two pumps indicated in the figure, then any power used to drive a pressure differential in the low to high pressure transition is recovered in the pump working the high to low pressure transition. For the molten salt case it is clear that one can do this with no additional power input over circulation requirements.

Finally, if there were to be a failure in either of the heat exchangers, or other components, then locking the drive shafts of the pump/motors would serve to isolate nuclear processes from chemical processes.

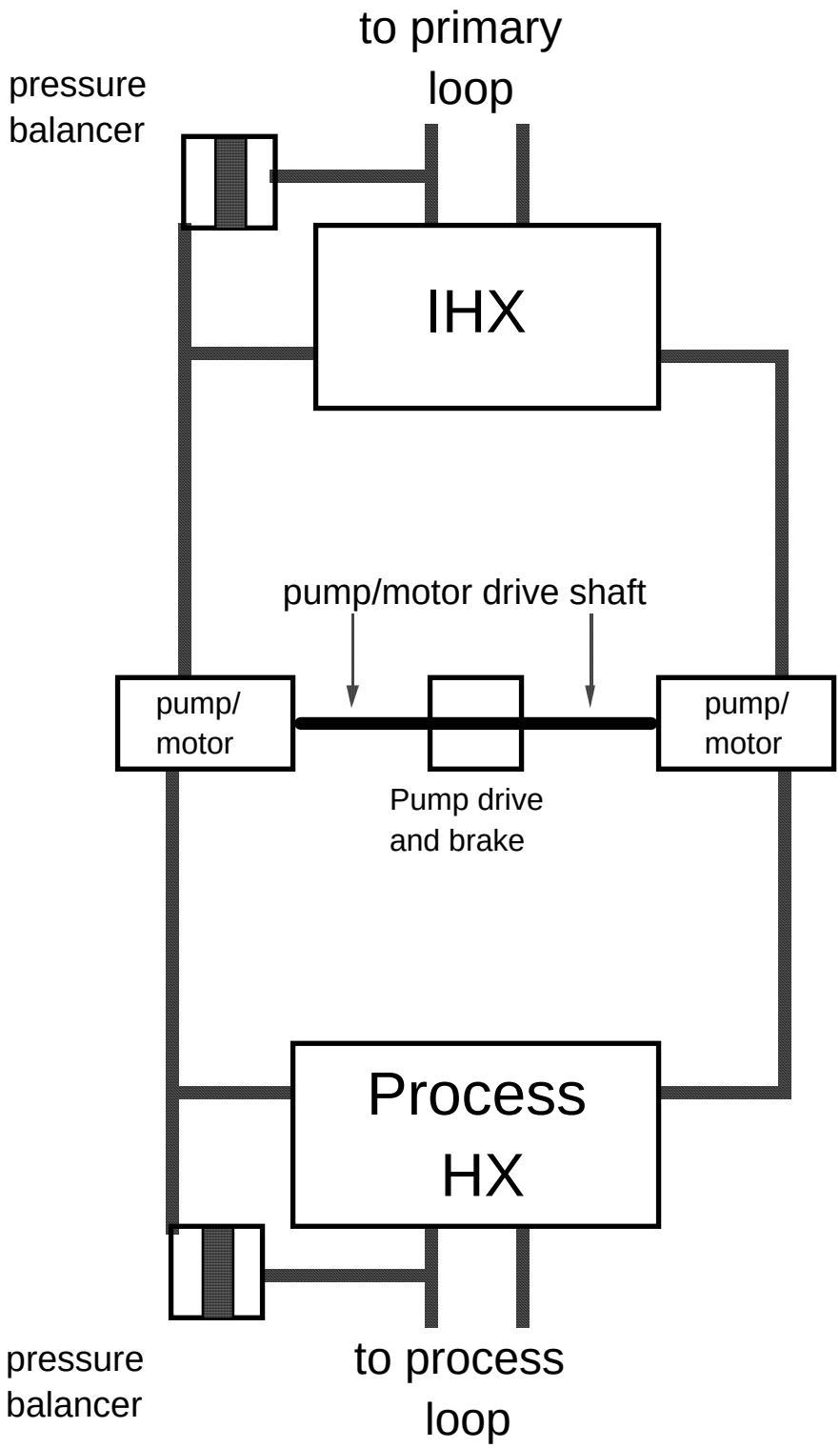

Figure 39. Suggestions for molten salt loop configuration.

6.0 The Development of Self Catalytic Materials for Thermochemical Water Splitting Using the Sulfur-Iodine Process (PI: Ronald Ballinger, MIT)

The national program had decided that the MIT program would be refocused. As a part of this refocus, the catalytic alloy development tasks were redefined to focus on the detailed characterization of the Pt-added alloys. The procurement and testing of a test article heat exchanger using the new alloys is being put on hold.

6.1 Material Chemistry Identification, Alloy Procurement and Metallurgical Characterization

New Alloys

As a part of the refocusing of the program, the new alloy characterization task will focus on a detailed characterization of the Pt-added alloys. While the test article production task (put on hold) would have required the production of larger (several 10s of kg) heats of material, detailed catalytic characterization will require much smaller amounts of material. In this case, the project can expand the number of Pt-added alloy combinations to better characterize the system. The proposed new work plan will focus on the following alloy compositions:

Alloy 800H + 1wt% Pt
Alloy 800H + 2wt% Pt
Alloy 800H + 5wt% Pt
Alloy 617 + 1wt% Pt
Alloy 617 + 2wt% Pt

Alloy melting was started this quarter in the Special Metals Corporation-Process Laboratory in New Hartford, NY. Each ingot weight is about 4 lbs, except for the alloy 800H+5 wt% Pt, which is 2 lbs. The expected completion date for the above set of alloy melting is January 15, 2007.

6.2 Catalyst Effectiveness Determination

Facility Construction

The catalyst facility is in operation. The manufacture's service contract for the GC unit is re-instated as of December 21, 2006. Currently, the GC unit is in the maintenance/repair process in anticipation of the work on the new heats of material.

6.3 Mechanical Properties Determination

The group is currently on schedule with the research plan in this task. However, this task will be redesigned based on the limited alloy mass that will be procured. As soon as the new materials are in house they will be characterized for catalytic activity as well as microstructure. Material will also be provided to INL for catalytic activity characterization.

7.0 Development of an Efficient Ceramic High Temperature Heat Exchanger (PI: Merrill Wilson, Ceramatec, Inc.)

7.1 Highlights

- The work associated with the FY06 work packages was completed. The report was sent in November.
- New work packages for bridge funding between FY06 and the receipt of FY07 funds were negotiated and signed in late November 2006.
- Samples of ceramic to ceramic joints were fabricated and are undergoing corrosion exposure testing. These exposures will be completed in January and readied for mechanical strength testing.

7.2 Technical Summary

Heat Exchanger Fabrication

Ceramatec has tape cast several lots of silicon carbide tape in order to build the inventory required for the fabrication of full-size heat exchanger plates. The designs to be fabricated are based on the Rev. 2.0 designs of FY2006 and subsequently of Rev 2.5 of this bridging program.

Heat Exchanger Joining

Joining samples were fabricated and corrosion testing began. These samples are being tested under high temperature air (900 C - baseline conditions) and under high temperature sulfuric acid/water/oxygen conditions. These samples were running for about 200 hours.

8.0 Efficiency Improvement and Cost Reduction of Solid Oxide Electrolysis Cells through Improved Electrodes and Electrolytes (PI: Clemens Heske, UNLV)

8.1 Introduction

The University of Nevada at Las Vegas (UNLV) and Argonne National Laboratory (ANL) have teamed up to address the underlying materials issues that affect the efficiency and cost-competitiveness of solid-oxide electrolysis cells (SOECs) for hydrogen production by high-temperature steam electrolysis. The project investigates structure-property-performance relationships for oxygen electrodes and electrolytes, as well as the fabrication of thin-film electrolytes using atomic layer deposition (ALD). The findings from this project will help with the design of higher efficiency, more durable, and less costly SOEC systems. The project draws on the unique combination of surface science and interface characterization capability at UNLV and leading-edge experience in fuel cell technology, electrochemical characterization, and ALD technology at ANL.

8.2 Research Accomplishments at UNLV

In the past quarter, the investigation of (La,Ca)MnO_3 (LCM) electrodes prepared by pulsed laser deposition (PLD), as well as Y-stabilized ZrO (YSZ) electrodes prepared by atomic layer deposition (ALD), continued. During the recent experimental run at the Advance Light Source at Lawrence Berkeley National Laboratory, x-ray absorption and x-ray emission spectra of those samples and suitable reference samples were collected.

A series of x-ray absorption spectra of LCM (left) and YSZ (right) films and corresponding references are shown in Figure 40 (note that the LCM figure includes some spectra taken in the ALS run in May 06 as well). The spectra show that x-ray absorption is a very sensitive tool to investigate the actual compound and oxidation state of the sample. The absorption spectra of the two LCM films on YSZ substrate exhibit an additional peak at around 532.2 eV compared to the spectrum of LCM on MgO. This additional peak can be attributed to a contribution of the YSZ substrate as the comparison with the YSZ absorption spectrum verifies. Note that when using the total fluorescence signal as a measure for the absorption as done in the present case the attenuation length is approximately 200 nm, and thus some signal from the YSZ electrolyte is seen "through" the electrode layer.

X-ray emission experiments were conducted in addition to the absorption measurements. Figure 41 shows the Y $M_{4,5}$ and Zr $M_{4,5}$ emission spectra of LCM and YSZ films, together with those of selected reference compounds. It was found that the Y $M_{4,5}$ emission of the YSZ films is in good agreement with that of the Y_2O_3 reference. Furthermore, as in the case of the x-ray absorption discussed above, the Y $M_{4,5}$ emission can also be observed "through" the LCM electrode. In contrast to the spectra of the bare YSZ sample an additional component in the x-ray emission spectrum was found pointing towards an interface component and/or intermixing at the interface.

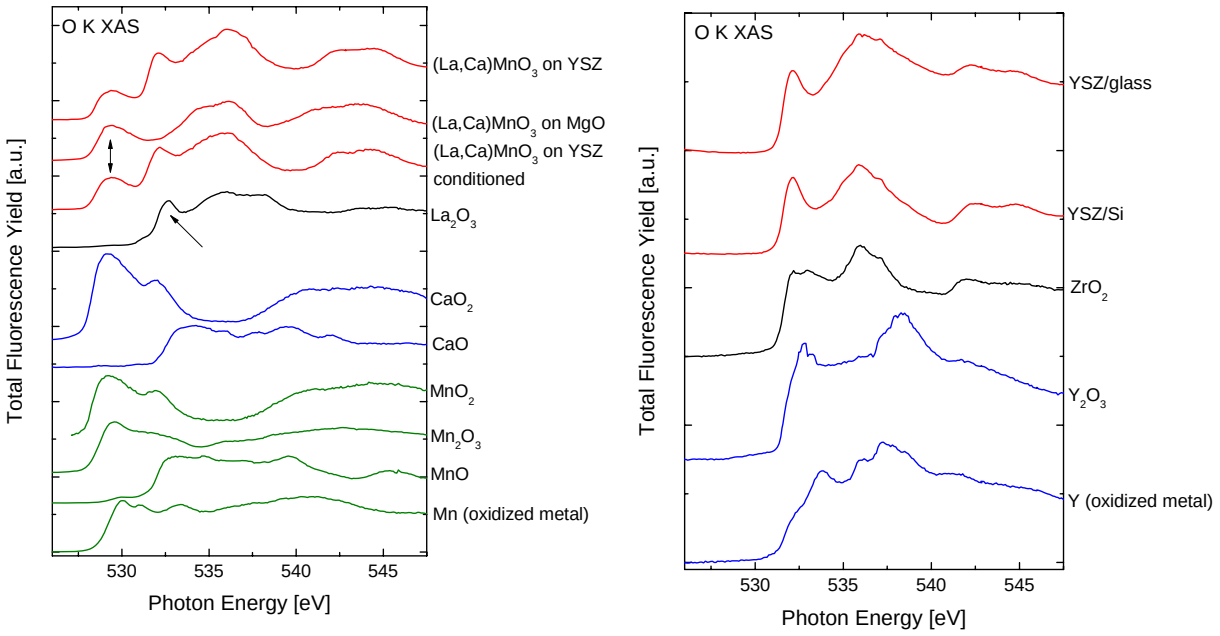

Figure 40. X-ray absorption spectra of LCM (left) and YSZ (right) films together with the spectra of several reference materials.

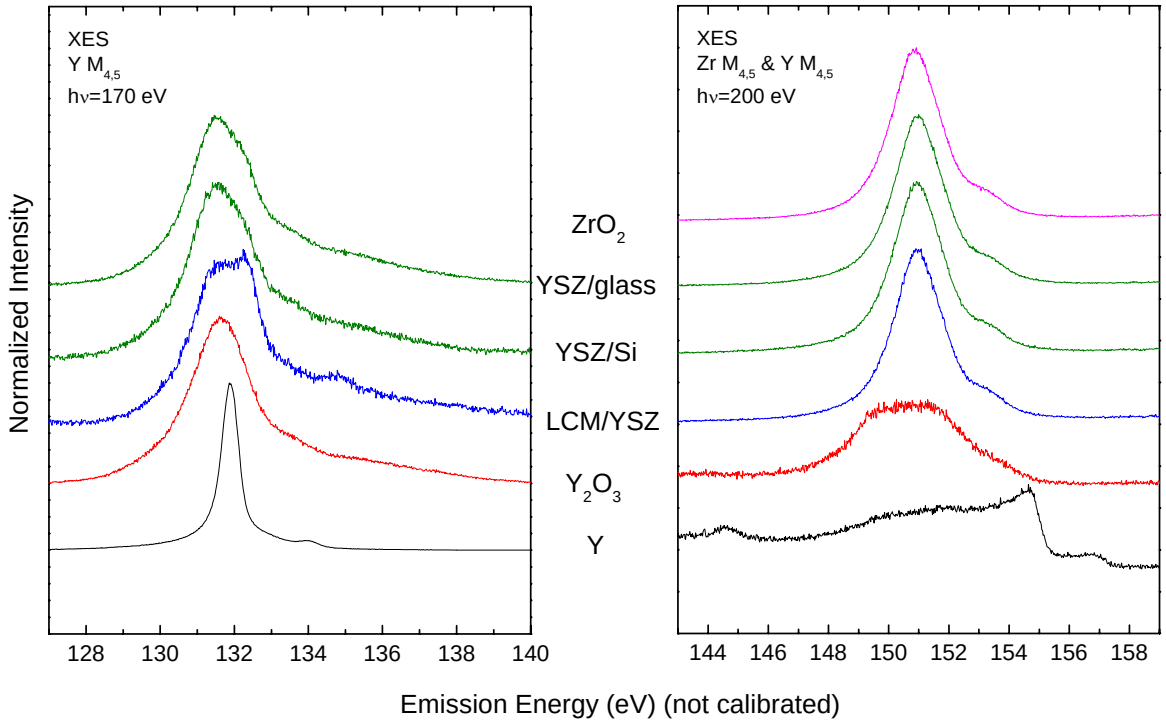

Figure 41. X-ray emission spectra of LCM and YSZ films together with those of some reference compounds.

Based on the results discussed above, and taking into account earlier photoemission measurements, a new series of samples was discussed with collaboration partners at ANL. The

main focus of these samples and experiments will be to elucidate the mechanism of electrochemical conditioning and its impact on the chemical and electronic surface properties of the LCM and LSM electrodes. Furthermore, Co-based LSC electrodes will be investigated.

8.3 Further Highlights

An ultra-high vacuum sample-heating stage was developed that allows to heat samples in vacuum and under oxygen gas environment. During the visit to ANL it was discussed that this capability would be important to modify surface properties and to simulate electrochemical condition steps performed at ANL. This heating stage was constructed, installed, and successfully commissioned. Temperatures up to 1400°C were achieved.

The graduate student on the project prepared and conducted the first experiments with the new scanning probe microscope. Once the above-mentioned samples are in hand, Atomic Force Microscopy images as well as selected Scanning Tunneling Spectra will be acquired.